Telegraphic switching signals by magnet tunnel junctions for neural spiking signals with high information capacity

Cite as: J. Appl. Phys. 124, 152121 (2018); https://doi.org/10.1063/1.5042444 Submitted: 31 May 2018 . Accepted: 07 August 2018 . Published Online: 02 October 2018

Brandon R. Zink, Yang Lv , and Jian-Ping Wang







ARTICLES YOU MAY BE INTERESTED IN

Chain of magnetic tunnel junctions as a spintronic memristor

Journal of Applied Physics 124, 152116 (2018); https://doi.org/10.1063/1.5042431

Ultra-fast logic devices using artificial "neurons" based on antiferromagnetic pulse generators Journal of Applied Physics 124, 152115 (2018); https://doi.org/10.1063/1.5042348

Perspective: Spintronic synapse for artificial neural network

Journal of Applied Physics 124, 151904 (2018); https://doi.org/10.1063/1.5042317







Telegraphic switching signals by magnet tunnel junctions for neural spiking signals with high information capacity

Brandon R. Zink, Yang Lv, and Jian-Ping Wang^{a)}
Department of Electrical and Computer Engineering, University of Minnesota, Minnesota, Minnesota 55455, USA

(Received 31 May 2018; accepted 7 August 2018; published online 2 October 2018)

Magnetic tunnel junctions (MTJs) operating in the superparamagnetic regime produce telegraphic signals that emulate neural spiking signals. Previous studies have characterized the random spiking signals produced by MTJs in terms of the percentage of time spent in the anti-parallel (AP) magnetization state (referred to as the "AP rate") but ignore the switching rate of the MTJ. In this work, we demonstrate that with proper tuning of both an external bias field and a bias voltage, we can control the average dwell time in the AP-state and P-state pulses separately. Our data show that the AP rate can be tuned with bias voltages ranging from 310 mV to 460 mV and bias fields from $-200 \, \text{Oe}$ to $-230 \, \text{Oe}$. The average dwell times in each state ranged from 225 ns to $285 \, \mu \text{s}$ and could be controlled separately. This suggests that neural spiking signals produced by MTJs can be decoded by both the spike rate and the spike count, which creates the possibility for increasing the information capacity in the rate coding scheme. *Published by AIP Publishing*. https://doi.org/10.1063/1.5042444

I. INTRODUCTION

Neuromorphic computing is a computing scheme that attempts to mimic methods in which biological nervous systems process information with the purpose of performing cognitive tasks such as pattern recognition, classification, and prediction. Their architectures consist of a network of nonlinear processing units called neurons, which receive and transmit electrical signals, which are modulated through synaptic weights. The computing model that most accurately emulates biological models is the neural spiking model² where information transmitted between neurons is represented by a temporal sequence of electrical pulses, or spiking signals. These spiking signals are decoded using a method called neural coding, which can implement either rate coding or temporal coding schemes. In rate coding, the spiking signals are averaged or by counting the number of spikes generated over a given measurement time,3 whereas temporal coding considers the precise timing of the spikes.^{3,4} Temporal coding methods have higher information capacity than rate coding schemes, 3,4 meaning that each spiking signal contains more information about the stimuli. However, rate coding methods have higher tolerance to noise since the spiking signals in rate coding schemes are assumed to be probabilistic.³

Magnetic tunnel junctions (MTJs) are promising devices for neuromorphic computing architectures due to their nonvolatility, non-linear dynamics, ultra-low power consumption, and scalability.^{5–7} Furthermore, MTJs exhibit tunable stochasticity due to thermal fluctuations, which is typically demonstrated through a synchronous process of consecutive write and read current pulses. These experiments have been done in order to test their reliability in spin-transfer torque switched magnetic random access memory (STT-MRAM)

cells^{8–10} as well as to demonstrate their function as true random number generators^{11,12} and stochastic computing units.¹³ Additionally, stochastic MTJs have been proposed as neurons and synapses in various stochastic spiking neuron circuits which implement a neural rate coding scheme.^{14–18} In these designs, some external stimuli (typically a current or voltage pulse) produces stochastic signals from the MTJs, which emulate neural spiking signals.

As the dimensions of the MTJ are scaled down, their stochasticity increases due to a decrease in thermal stability. Eventually, the energy barrier separating the anti-parallel (AP) and parallel (P) states drops below 5 k_bT, at which point the MTJ reaches a superparamagnetic state 19 and thermal fluctuations will cause the free layer magnetization to randomly switch between the two resistance states. This generates time-domain telegraphic signals, which can be tuned using a bias current or a bias field and are characterized by the percentage of time the MTJ spends in both states or the average dwell time in each state. ^{20,21} Superparamagnetic MTJs have been demonstrated to exhibit stochastic resonance when exposed to a weak, external AC signal, 22 suggesting that these devices could be implemented in stochastic oscillator neural networks.^{23,24} Low-barrier MTJs also present a unique opportunity for ultra-low power, spin-based computing platforms called probabilistic spin logic (PSL) where novel circuits such as invertible Boolean logic circuits, ^{25,26} Bayesian networks,²⁷ and resistive-deep belief networks²⁸ have been proposed in recent years.

Several recent studies have explored telegraphic signals generated by low-barrier MTJs as neural spiking signals. 19,29,30 Experimental results produced by Suh *et al.* 30 demonstrated that a neuron-synapse system can be formed using a low-barrier MTJ as a neuron and memristive MTJ as the synapse. Telegraphic switching signals in the MTJ were controlled via the application of a DC voltage bias and a field bias (V_{bias} and H_{bias} , respectively). A rate coding

^{a)}Author to whom correspondence should be addressed: jpwang@umn.edu

scheme was realized by measuring the average firing rate, which was represented by the percentage of measurement time the MTJ spent in the AP state, which will be referred to as the "AP rate."

In this work, we expand on the work done by Suh *et al.* by demonstrating separate control over the average AP- and P-state pulse widths ($\langle \tau_{AP} \rangle$ and $\langle \tau_{P} \rangle$, respectively). This indicates that the AP rate and the number of AP pulses can be treated as independent variables, which suggests that the neuron-synapse system tested by Suh *et al.* is capable of implementing a rate coding scheme with two degrees of freedom. These findings open the possibility for rate coding schemes with increased information capacity.

II. EXPERIMENT

Testing was performed on an MTJ with a nanopillar stack and an elliptical cross section with nominal dimensions of $45 \times 110 \,\mathrm{nm^2}$. The stack structure of the MTJ is PtMn (15)/SAF/MgO (0.85)/Co₂₀Fe₆₀B₂₀ (1.8), where the thicknesses given are in units of nm and the SAF (synthetic antiferromagnet) layers have a structure of Co₇₀Fe₃₀ (2.3)/Ru (0.85)/Co₄₀Fe₄₀B₂₀ (2.4). The device has a resistance-area product of $4.3 \,\Omega \,\mu\mathrm{m^2}$, a coercivity of 23.5 Oe, and a tunneling magnetoresistance (TMR) ratio of 106%, where the resistances in the AP and P states of 3300 Ω and 1600 Ω , respectively. The hysteresis plot for our MTJ is shown in Fig. 1.

The MTJ tested is thermally stable at zero bias and room temperature; however, we induced telegraphic signals using a field and voltage bias (illustrated in the inset of Fig. 1). Note that our method is very similar to the one used by Suh et al.³⁰ At thermal equilibrium, the energy band diagram with respect to orientation of magnetization of the free layer (M_f) will be symmetric between the AP- and P-states. When a bias field is applied in the direction that favors P-state orientation, the energy increases in the AP-state and decreases in the P-state. This reduces the energy barrier seen in the AP-state and increases the barrier seen in the P-state. The opposite effect happens when a positive bias voltage is applied; the resulting spin-polarized current through the MTJ produces a spin-torque term which favors the AP-state

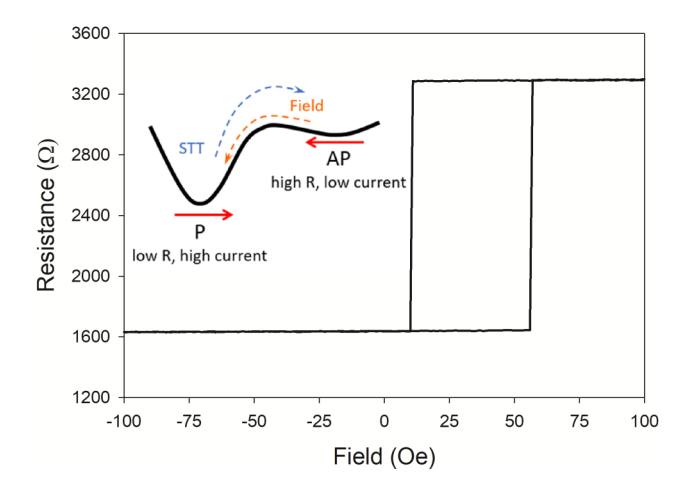


FIG. 1. Hysteresis loop for the MTJ tested and an illustration of the energy barrier in the AP- and P-states (inset).

orientation. We observed that telegraphic signals were generated when the energy barrier of the MTJ was less than 8 k_bT.

It should be noted that the shape of the energy band diagram is not the same when the MTJ is in the AP and P states. This is because the resistance in the AP state is higher than in the P state, and since $V_{\rm bias}$ is constant, the current through the MTJ is higher in the P-state. A higher current means a more significant reduction in the energy barrier in the P-state, resulting in a higher probability of P to AP switching. After the MTJ switches to the AP state, the current is reduced, thus reducing the energy barrier in the AP-state, which allows for a higher probability of AP to P switching from $H_{\rm bias}$.

Measurements were made on a Tektronix DPO 72004C mixed signal oscilloscope, the bias voltage was provided using a Keithley 2400 source meter, and the bias field was generated using a Kepco BOP 20-20 power supply. A series connection was made between the MTJ and the oscilloscope, which has an internal resistance of $50\,\Omega$. In effect, the MTJ created a voltage divider network with the $50\,\Omega$ internal resistance of the oscilloscope. The voltage measured at the oscilloscope was used to calculate the resistance of the MTJ at each data point. Each trial was measured for 2 ms in 80 ps intervals.

III. RESULTS

Data sets were taken at bias fields of -200, -215, and -230 Oe and bias voltages ranging from 310 mV to 460 mV. Figure 2 shows the telegraphic signals for four of these sets. The numbers displayed above each set in Fig. 2 are given in the order H_{bias} , V_{bias} , AP rate, $\langle \tau_{\text{AP}} \rangle$, and $\langle \tau_{\text{P}} \rangle$. Trials (a) and (b) have roughly the same V_{bias} but trial (a) has a larger

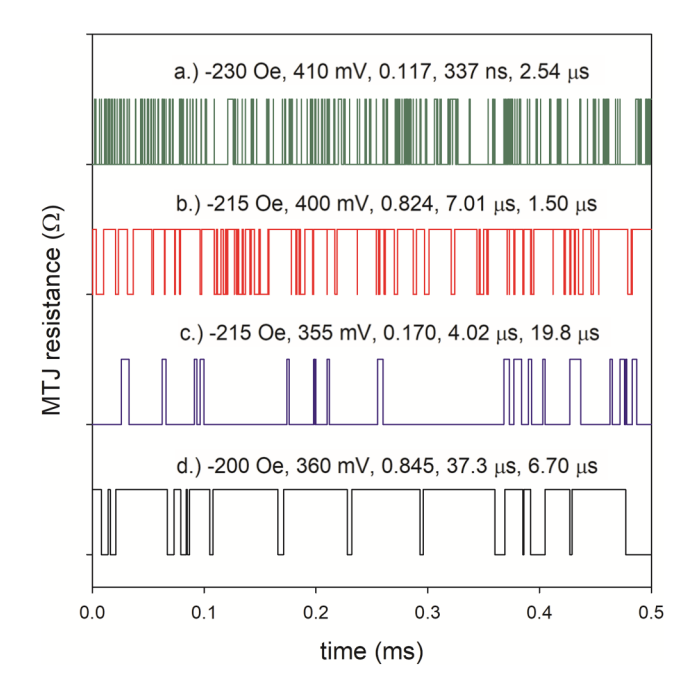


FIG. 2. Four different telegraphic switching signals produced by the MTJ under varying bias conditions. The set of numbers above each set indicate the bias conditions and the key measurements. These numbers follow the order H_{bias} , V_{bias} , AP rate, $<\tau_{\text{AP}}>$, and $<\tau_{\text{P}}>$.

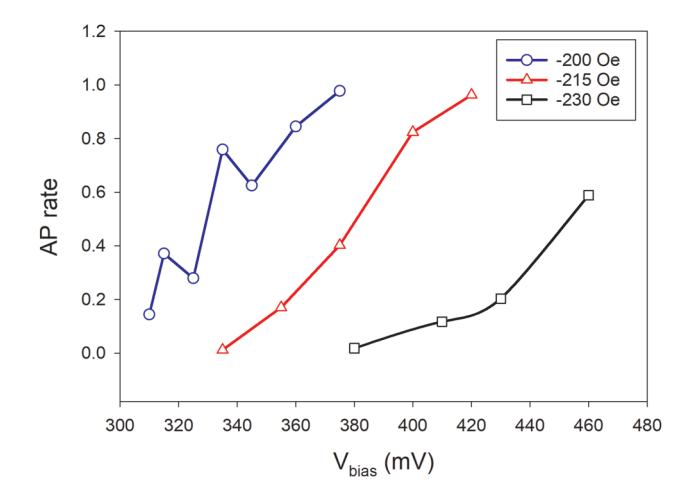


FIG. 3. AP rate versus V_{bias} for the three H_{bias} values tested.

 $H_{\rm bias}$. Therefore, it is unsurprising, the trial (a) has a smaller AP-rate, since $H_{\rm bias}$ is set to favor the P-state. The same observation can be made when comparing trials (c) and (d). Conversely, trials (b) and (c) have the same $H_{\rm bias}$, but trial (b) has a larger $V_{\rm bias}$. As seen in Fig. 2, trial (b) has a larger AP-rate, which is expected since $V_{\rm bias}$ is set to favor the AP-state.

The overall effect of how the AP rate is affected by V_{bias} for a constant H_{bias} is illustrated in Fig. 3. This plot indicates a trade-off between low bias voltages and a large tunability range in V_{bias} . With lower H_{bias} values, telegraphic switching signals can be generated at lower bias voltages. However, this also means that the AP rate is tunable through a smaller range of bias voltages. The data from Fig. 3 demonstrate that the AP rate can be tuned from 0 to 1 through a 65 mV range of bias voltages for $H_{bias} = -200$ Oe. This range increases to

85 mV for $H_{\text{bias}} = -215 \text{ Oe}$ and 80 mV for $H_{\text{bias}} = -230 \text{ Oe}$. However, the AP rate for the -230 Oe trials is only tuned from 0 to 0.6. Higher ranges of tunability allow for more precise control of the MTJ output, thus higher resolution measurements can be made.

The tunability of the AP rate is not unexpected and has already demonstrated in several previous experiments. 20,21,30 However, interesting results from our data are seen in the relation between H_{bias} and V_{bias} versus $<\tau_{AP}>$ and $<\tau_{P}>$. Returning to the trials shown in Fig. 2, we see that $\langle \tau_{AP} \rangle$ in trial (a) is over 1 order of magnitude lower than in trial (b), yet $\langle \tau_p \rangle$ in trials a and b are roughly the same. Recall that these two trials have roughly the same V_{bias} but differ in H_{bias} , and we can see that the trial with the larger H_{bias} has a significantly smaller $\langle \tau_{AP} \rangle$. Furthermore, $\langle \tau_{AP} \rangle$ for trials (b) and (c) are on the same order of magnitude; however, $\langle \tau_P \rangle$ is significantly larger in trial (c). As previously stated, these trials have the same H_{bias} , but trial (b) has a larger V_{bias} . These observations indicate that $\langle \tau_P \rangle$ has a stronger dependence on the bias voltage than it has on the bias field, whereas $\langle \tau_{AP} \rangle$ has a stronger dependence on bias field.

These observations are further substantiated when we consider the range of $\langle \tau_{AP} \rangle$ and $\langle \tau_{P} \rangle$ for each H_{bias} set shown in Fig. 3. The values of $\langle \tau_{AP} \rangle$ range from 37.3 to 89.9 μ s, 2.05 to 10.8 μ s, and 255 to 366 ns for the -200, -215, and -230 Oe sets, respectively. The upper end of these ranges were generated in trials with larger V_{bias} values; however, note that $\langle \tau_{AP} \rangle$ does not change orders of magnitudes if H_{bias} is held constant. On the other hand, $\langle \tau_{P} \rangle$ values range from 1.51 to 285 μ s, 418 ns to 188 μ s, and 255 ns to 15.4 μ s for the H_{bias} sets at -200, -215, and -230 Oe sets, respectively. While $\langle \tau_{P} \rangle$ tended to decrease between sets with larger H_{bias} , the change between sets was much more significant than the variation within each set. The range of $\langle \tau_{P} \rangle$

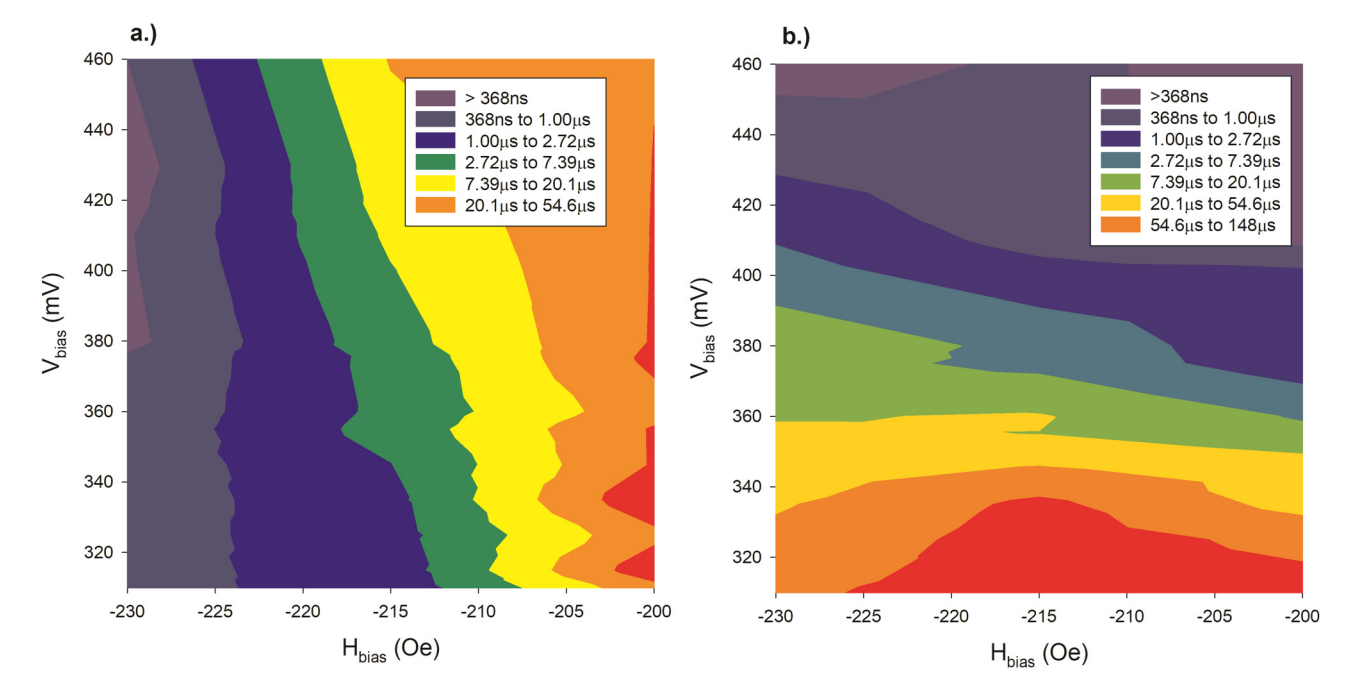


FIG. 4. Contour map of the average pulse widths over all bias voltages and bias fields for (a) the AP-states and (b) the P-states. These contour maps are displayed on a natural logarithmic scale.

TABLE I. Correlation coefficients between the biases and the average AP- and P-state pulse widths (natural log scale).

	H_{bias}	V _{bias}
$ln(<\tau_{AP}>)$	0.979	-0.793
$ln(<\!\!\tau_P\!\!>)$	0.565	-0.945

decreased by 1 order of magnitude between the H_{bias} sets; however, $\langle \tau_P \rangle$ varied by at least 3 orders of magnitude within each set.

The AP- and P-state pulse widths are mapped out in Figs. 4(a) and 4(b), which show logarithmic-scale contour plots of $\langle \tau_{AP} \rangle$ and $\langle \tau_{P} \rangle$ versus V_{bias} and H_{bias} . Figure 4(a) displays the AP-state pulse widths, where the contour lines of $\langle \tau_{AP} \rangle$ run mostly parallel to the V_{bias} axis and perpendicular to the H_{bias} axis. The opposite relation is shown for the P-state pulse widths in Fig. 4(b), where the contour lines of $\langle \tau_P \rangle$ run perpendicular to the V_{bias} axis and parallel to the H_{bias} axis. As previously stated, V_{bias} has an effect on $\langle \tau_{AP} \rangle$ and H_{bias} has an effect on $\langle \tau_P \rangle$. However, these relations are not significant (seen in Table I), which show the correlation coefficients for H_{bias} and V_{bias} in relation to $ln(<\tau_{AP}>)$ and $ln(\langle \tau_P \rangle)$. These correlation coefficients further demonstrate that H_{bias} and V_{bias} have very asymmetric effects on $\langle \tau_{AP} \rangle$ and $\langle \tau_P \rangle$. Remember that these correlations are calculated on a natural log-scale for $\langle \tau_{AP} \rangle$ and $\langle \tau_{P} \rangle$, meaning that even if changes in H_{bias} produced changes in $\langle \tau_P \rangle$, the change in $\langle \tau_{AP} \rangle$ could be as high as 3 orders of magnitude higher than the change in $\langle \tau_P \rangle$, as seen from our data. The same statement can be made for the effect of changes in V_{bias} on $\langle \tau_{AP} \rangle$.

This discrepancy in how the two biases effect $\langle \tau_{AP} \rangle$ and $\langle \tau_{P} \rangle$ separately allows for independent control over the AP rate and the number of AP pulses generated. What this feature implies for rate coding is that the average spike rate and the spike count are no longer separate decoding methods, but now are independent variables that can be considered separately in the same decoding scheme. Using MTJs in the telegraphic switching regime introduces the potential for increasing the information capacity in the rate coding scheme.

A significant shortcoming to this method is that it requires a tunable external field. Not only is this not practical for neuromorphic computing designs but applying a bias field also requires large power consumption. For this reason, future work should be focused on improving this method by eliminating the need for a bias field. Other alternatives, such as magneto-electric coupling, should be explored.

IV. CONCLUSIONS

In this work, we demonstrated that through proper tuning of the bias field and voltage, MTJs can generate tunable telegraphic switching signals, which emulate neural spiking signals. These devices can be used to implement a rate coding scheme where the average spike rate is represented by the AP rate, which can be easily tuned with external parameters, which in our case were a bias field

and a bias voltage. Furthermore, our data show that the average AP-state pulse width could be controlled separately from the average P-state pulse width, meaning that the number of AP pulses generated is independent of the AP-rate with this method. This introduces the possibility for a rate coding scheme to be implemented where the spike rate and the spike count are independent of each other. A rate coding scheme with this feature would have higher information capacities while maintaining their noise tolerance.

ACKNOWLEDGMENTS

This work is supported in part by the Center for Probabilistic Spin Logic for Low-Energy Boolean and Non-Boolean Computing (CAPSL), one of the Nanoelectronic Computing Research (nCORE) centers as task 2759.001, and a Semiconductor Research Corporation (SRC) program sponsored by the National Science Foundation (NSF) through 1739635.

¹Y. LeCun, Y. Bengio, and G. Hinton, Nature **521**, 436 (2015).

²C. Mead, *Analog VLSI and Neural Systems* (Addison-Wesley, Reading, MA, 1989).

³T. U. Krautz, M.S. thesis, Ruhr-University Bochum, 2014.

⁴H. Paugam-Moisy and S. Bohte, "Computing with spiking neuron networks," in *Handbook of Natural Computing*, edited by G. Rozenberg, T. Bäch, and J. N. Kik (Springer, Berlin, Heidelberg, 2012), pp. 335–376.
 ⁵J. Grollier, D. Querlioz, and M. D. Stiles, Proc. IEEE 14, 2024 (2016).

⁶N. Locatelli, A. F. Vincent, A. Mizrahi, J. S. Friedman, D. Vodenicare, J.-V. Kim, J.-O. Klein, W. Zhao, J. Grollier, and D. Querlioz, in Proceedings of the Design, Automation, and Test in Europe Conference and Exhibition, Grenoble, France, April 2015, pp. 994–999.

⁷J.-P. Wang, S. S. Sapatnekar, C. H. Kim, P. Crowell, S. Koester, S. Datta, K. Roy, A. Raghunathan, X. S. Hu, M. Niemier, A. Naeemi, C.-L. Chien, C. Ross, and E. Kawakami, in Proceedings of the Design Automation Conference, Austin, TX, USA, June 2017.

⁸H. Zhao, A. Lyle, Y. Zhang, P. K. Amiri, G. Rowlands, Z. Zeng, J. Katine, H. Jiang, K. Galatsis, K. L. Wang, I. N. Krivorotov, and J.-P. Wang, J. Appl. Phys. **109**, 07C720 (2011).

⁹H. Zhao, Y. Zhang, P. K. Amiri, J. Katine, J. A. Langer, H. Jiang, I. N. Krivorotov, K. L. Wang, and J.-P. Wang, IEEE Trans. Magn. 48, 3818 (2012).

¹⁰T. Aoki, Y. Ando, M. Oogane, and H. Naganuma, Appl. Phys. Lett. **96**, 142502 (2010).

¹¹W. H. Choi, Y. Lv, J. Kim, A. Deshpande, G. Kang, J.-P. Wang, and C. H. Kim, in IEEE International Electron Devices Meeting, San Francisco, CA, USA, December 2014, pp. 12.5.1–12.5.4.

¹²A. Fukushima, T. Seki, K. Yakushiji, H. Kubota, H. Imamura, S. Yuasa, and K. Ando, Appl. Phys. Exp. 7, 083001 (2014).

¹³Y. Lv and J.-P. Wang, in IEEE International Electron Devices Meeting, San Francisco, CA, USA, December 2017, pp. 36.2.1–36.2.4.

¹⁴G. Srinivasan, A. Sengupta, and K. Roy, in Proceedings of the Design, Automation, and Test in Europe Conference and Exhibition, Lausanne, Switzerland, March 2017, pp. 530–535.

¹⁵A. Sengupta, M. Parsa, B. Han, and K. Roy, IEEE Trans. Electron Devices 63, 2963 (2016).

¹⁶D. Zhang, L. Zeng, Y. Zhang, W. Zhao, and J. O. Klein, in IEEE/ACM International Symposium on Nanoscale Architectures, Beijing, China, July 2016, pp. 173–178.

¹⁷A. Sengupta, P. Panda, P. Wijesinghe, Y. Kim, and K. Roy, Sci. Rep. 6, 30039 (2016).

¹⁸D. Zhang, L. Zeng, F. Gong, T. Gao, S. Gao, Y. Zhang, and W. Zhao, in 15th Non-Volatile Memory Technology Symposium, Beijing, China, October 2015, pp. 1–4.

¹⁹C. M. Liyanagedera, A. Sengupta, A. Jaiswal, and K. Roy, Phys. Rev. Appl. 8, 064017 (2017).

²⁰M. R. Pufall, W. H. Rippard, S. Kaka, S. E. Russek, and T. J. Silva, Phys. Rev. B 69, 214409 (2004).

- ²¹X. Cheng, C. T. Boone, J. Zhu, and I. N. Krivorotov, Phys. Rev. Lett. **105**, 047202 (2010).
- ²²N. Locatelli, A. Mizrahi, A. Accioly, R. Matsumoto, A. Fukushima, H. Kubota, S. Yuasa, V. Cros, L. G. Pereira, D. Querlioz, J.-V. Kim, and J. Grollier, Phys. Rev. Appl. 2, 034009 (2014).
- ²³ A. Mizrahi, N. Locatelli, R. Matsumoto, A. Fukushima, H. Kubota, S. Yuasa, V. Cros, J.-V. Kim, J. Grollier, and D. Querlioz, IEEE Trans. Magn. 51, 11 (2015).
- ²⁴A. Mizrahi, N. Locatelli, J. Grollier, and D. Querlioz, Phys. Rev. B 94, 054419 (2016).
- ²⁵K. Y. Camsari, R. Faria, B. M. Sutton, and S. Datta, Phys. Rev. X 7, 031014 (2017).
- ²⁶R. Faria, K. Y. Camsari, and S. Datta, IEEE Magn. Lett. **8**, 1 (2017).
- ²⁷R. Faria, K. Y. Camsari, and S. Datta, AIP Adv. **8**, 045101 (2018).
- ²⁸R. Zand, K. Y. Camsari, I. Ahmed, S. D. Pyle, C. H. Kim, S. Datta, and R. F. DeMara, preprint arXiv:1710.00249 (2017).
- ²⁹P. Krzysteczko, J. Munchenberger, M. Schafers, G. Reiss, and A. Thomas, Adv. Mater. 24, 762 (2012).
- ³⁰D. I. Suh, G. Y. Bae, H. S. Oh, and W. Park, J. Appl. Phys. **117**, 17D714 (2015).